International Journal of Numerical Methods for Heat & Fluid Flow

3749

Received 28 January 2025
Revised 23 May 2025
Accepted 14 June 2025

Numerical modelling and experimental validation of heat transfer enhancement and thermal mixing in a triple-tube heat exchanger for food processing

Luca Pagliarini, Umberto Neviani and Sara Rainieri
Department of Engineering and Architecture Parco Area delle Scienze, University of Parma, Parma, Italy

Abstract

Purpose – The aim of this study is to evaluate the thermal performance of a triple-tube heat exchanger equipped with staggered fins for food processing. Challenges arise due to the high viscosity of non-Newtonian fluids treated in the food industry, which lead to laminar flow and limited thermal penetration. This research focuses on enhancing heat transfer efficiency and improving fluid thermal mixing using passive heat transfer enhancement methods in a triple-tube heat exchanger.

Design/methodology/approach – Numerical simulations, implemented within an ANSYS© Fluent environment, are used to solve the equations governing the thermofluid dynamics of a triple-tube heat exchanger with staggered fins in the internal annulus. The rheological behavior of tomato concentrate is modeled by means of a power-law model, coupled with the Arrhenius law to introduce temperature dependency of the consistency index. Experimental validation is adopted to verify simulations accuracy.

Findings – The finned configuration enhances heat transfer and improves thermalization by induced swirling flows and consequent boundary layers disruption. The geometrical configuration presenting eight-finned modules achieves a maximum performance index of 1.23 in the entrance region, while mitigating frictional effects. Moreover, such fins arrangement guarantees good thermal mixing.

Originality/value – This study represents one of the first attempts of enhancing heat transfer performance of a triple-tube heat exchanger for thermal processing of food products. The exceptionally low generalized Reynolds number and high generalized Prandtl number characterizing the treated fluid result in severe heat transfer limitations, tackled by a practical design strategy able to improve energy and thermal treatment efficiency.

Keywords Computational fluid dynamics (CFD), Food processing, Passive heat transfer enhancement, Thermal mixing, Triple-tube heat exchangers

Paper type Research paper

Nomenclature

A = Constant (Pa s^n);
A_{tot} = Total heat transfer area (m^2);
Br_g = Generalized Brinkman number;

Competing interests: No competing interests were disclosed.

International Journal of Numerical Methods for Heat & Fluid Flow
Vol. 35 No. 11, 2025
pp. 3749-3774
Emerald Publishing Limited
0961-5539
DOI 10.1108/HFF-01-2025-0058

c_p = Specific heat (J/kg K);
d = Distance between finned modules (m);
D_h = Hydraulic diameter (m);
D_i = Inner diameter (m);
D_o = Outer diameter (m);
E_a = activation energy (J/mol);
f = Friction factor;
h = Convective heat transfer coefficient (W/m^2K);
K = Consistency index ($Pa\ s^n$);
k = Thermal conductivity (W/mK);
L = Length of the triple-tube passage (m);
l = Length of the finned module (m);
L_c = Curvilinear length of the sterilizer curve (m);
$\dot{m}$ = Mass flow rate (kg/s);
$\hat{n}$ = Unity vector (m);
n = Flow behavior index;
Nu = Nusselt number;
PD = Percentage deviation (%);
Pr_g = Generalized Reynolds number;
Q = Heat transfer rate (W);
R = Universal gas constant (J/mol K);
Re_g = Generalized Reynolds number;
T = Temperature (K);
$\boldsymbol{u}$ = Velocity vector (m/s);
W = Average velocity (m/s);
x = Axial coordinate (m);
α = Thermal diffusivity (m^2/s);
$\dot{\boldsymbol{\gamma}}$ = Rate-of-strain tensor (1/s);
ΔT_{ml} = Logarithmic mean temperature difference (K);
δ = Uncertainty;
η = Performance index;
η_a = Apparent viscosity (Pa s);
θ = Dimensionless temperature;
ρ = Density (kg/m^3);
$\boldsymbol{\tau}$ = Shear stress tensor (Pa);
σ = Temperature standard deviation (K); and
ψ = Mixing parameter.

Subscripts and superscripts

$*$ = Dimensionless;
b = Bulk;
c = Cold;
f = Fluid;
h = Hot;
in = Section inlet;
out = Section outlet;
s = Solid;
$wall$ = Wall properties; and
0 = Reference conditions.

1. Introduction

Innovation in the food machinery sector is currently driven by the demand for novel food processing techniques – both thermal and nonthermal – that ensure microbiological and chemical safety while preserving nutritional content and sensory qualities. At the same time, these processes must minimize energy consumption, thereby reducing the environmental impact of the entire food chain (Chakka *et al.*, 2021).

A key element in food thermal processing is the Heat Exchanger (HE). This equipment must comply with strict safety standards to effectively inactivate microbes while maintaining the food's nutritional and sensory properties. The design and optimization of HEs are critical: achieving uniform heat distribution, preventing contamination and minimizing thermal degradation are all essential goals (Tonyali Karsli and Cekmecelioglu, 2023).

These problems, which refer to forced convection heat transfer within internal flow configurations, imply the selection of a suitable passive enhancement strategy, a choice that is highly dependent on the established flow regime, primarily influenced by the fluid's rheological properties and the geometrical features. When the laminar flow regime limiting boundaries cannot be overcome, the only possibility to passively enhance the heat transfer phenomenon is associated with solutions that force the fluid mixing, such as flow inserts (Bozzoli *et al.*, 2021; Pagliarini *et al.*, 2024a), twisted tapes (Zimparov *et al.*, 2024) or other solutions aimed at promoting swirl flow components (Rainieri and Pagliarini, 2002). These additional geometrical solutions improve fluid thermalization without requiring external power (Bozzoli *et al.*, 2020), but not all the listed methods are suitable for the food sector because fouling phenomena must be prevented or at least minimized (Schnöing *et al.*, 2020). Another challenge arises from the complex rheological behavior exhibited by many food products, which is often associated with the laminar flow regime due to the high consistency index of food products (Myhan *et al.*, 2012).

Heat transfer capability optimization relies on accurate modeling of the complex thermal fluid dynamics within the HE system. Advanced Computational Fluid Dynamics (CFD) simulations and predictive algorithms allow for detailed analysis of flow patterns and temperature distributions. By systematically adjusting geometric parameters, it becomes possible to quantify and implement improvements in heat transfer performance, comparing enhanced configurations to a baseline design [see, for instance, Vocale *et al.* (2019)]. The combination of experimental and numerical pieces of information becomes thus necessary for approaching the best strategy for topological and morphological optimization of the heat transfer sections with the aim of increasing the overall energy efficiency of industrial equipment (Bhattacharyya *et al.*, 2022). Recent works dealing with the numerical analysis of heat transfer augmentation solutions in HEs via commercial software can be found, for instance, in Abbasian Arani and Moradi (2021) and Aytaç *et al.* (2023).

The above consideration holds for both double-pipe and triple-tube HEs (TTHEs). In particular, the latter systems stand as highly advantageous heat transfer systems, especially when the treated fluid presents high viscosity and complex rheological behavior, such as in the food thermal processing (García-Valladares, 2004; Malavasi *et al.*, 2021). TTHEs present an additional annular passage, which consequently increases the heat transfer area. Large temperature gradients in the fluid are mitigated by such a geometrical configuration, thanks to its intrinsic capability of controlling the temperature difference between the process and the service fluids. Hence, enhancing heat transfer in TTHEs by means of passive methods is crucial to obtain even more efficient and cost-effective solutions for food processing.

While passive heat transfer enhancement methods for double-pipe HEs have been widely studied, only recently scholars have extended their application to the internal annulus of

TTHEs by also relying on numerical approaches, given the practical unfeasibility of experimentally monitoring all the thermofluidic features of the treated flows.

Gomaa *et al.* (2017) were among the firsts to experimentally and numerically study the effect of rib inserts on the performance of a TTHE for hot water cooling. Different geometrical parameters were considered, including varying heights and pitches of ribs. Simulations were carried out to shed light on the thermofluid dynamics characterizing the system. The Nusselt number was assessed to undergo an increase of 21.48% with respect to the nonfinned geometry. The heat transfer per unit pumping power exhibited an increase of 32.49% for the counter flow. Higher ribs height and low pitch resulted in a slight increase in the internal annulus heat transfer coefficient, when compared to the resulting increased pressure drops. Bahiraei *et al.* (2021a) proposed novel crimped-spiral ribs in the internal annulus of a TTHE and nanofluids for heat transfer improvement. The flow was characterized by a Reynolds number greater than 2,000. Numerical solutions were obtained through the two-phase mixture method. Turbulent flow was modeled by the Reynolds Stress Model. Different heights and pitches of the ribs were explored. Numerical data were validated against the data by Gomaa *et al.* (2017). The employment of higher height and pitch led to a significant increase in the heat transfer capability of the system (enhancement in heat transfer coefficient higher than 35.65%), contrarily to what reported in Gomaa *et al.* (2017). In addition, increment in nanofluid volume fraction of 0.02 resulted in an increment of overall heat transfer coefficient of 44.91%. The heat transfer augmentation achieved through geometrical characteristics of ribs and nanoparticle concentration agreed with that reported by Bahiraei *et al.* (2019) in turbulent flow condition. The heat transfer rate of a ribbed TTHE operating with nanofluids was therefore predicted with good accuracy by Bahiraei *et al.* (2021b) through an artificial neural network approach, coupled with the ant lion optimizer, by performing numerical simulations. Tiwari *et al.* (2021) analyzed, through experiments and CFD, the effects of a turbulent WO3/water nanofluid flow and different inserts on the thermal performance of a TTHE. The investigated geometries were rib inserts, twisted tape inserts and porous plate inserts. The numerical results highlighted increments of 12.38%, 11.83% and 8.61% in overall heat transfer coefficient were achieved using rib, porous plate and twisted tape inserts, respectively, with respect to the nonfinned geometry. The authors additionally underlined the urgent need for size optimization of the HE by using various novel inserts.

In the light of the provided literature, research effort has been focusing on heat transfer augmentation of TTHEs, despite the number of studies and research groups involved is still extremely limited. Moreover, to the authors' best knowledge, solutions for the food processing field in TTHEs are not yet proposed and analyzed because investigations mainly deal with turbulent flows of water or nanofluids. Such a lack of outcomes on TTHEs and their optimization has also been pointed out by the recent review works by Mukesh Kumar and Hariprasath (2020) and Akgul *et al.* (2023). Established performance enhancement techniques for TTHEs are thus still far from being achieved, undermining proper design and application. From the applicative point of view, such a limited offer of heat transfer augmentation solutions in the field of food thermal treatment via TTHEs leads to the usual employment of high safety factors, eventually undermining plants efficiency at the expense of poorer product quality and higher environmental impact (higher energy and water consumption) (Kubo *et al.*, 2023).

The aim of the present work is to fill this literature gap by studying a novel geometry for heat transfer enhancement in TTHEs for food processing, capable of ensuring both enhanced heat transfer and good fluid thermalization in laminar flows. The internal annulus of the investigated TTHE is equipped with modules of staggered, interrupted helical fins to induce swirling flow and boundary layer disruption. The novel design for heat transfer augmentation in TTHEs comes from the idea of revisiting classical geometries, extensively studied in the

field of double-pipe HEs for higher heat transfer efficiency and fluid mixing. In particular, the beneficial effects of classical helical fins, i.e. lower pressure drops with resulting lower heat transfer coefficients (Mozafarie and Javaherdeh, 2019), are here integrated with those of interrupted fins configurations, i.e. higher heat transfer coefficients with resulting higher pressure drops due to higher flow disturbances (El Maakoul *et al.*, 2020). The present hybrid geometry is thus believed to promote better fluid mixing and overall heat transfer performance during the operation of TTHEs, while mitigating the resulting pressure drops. A numerical approach is used to provide an in-depth and robust insight into the complex thermal fluid dynamic phenomena occurring within the system. The CFD model, implemented within an ANSYS© Fluent environment, is experimentally validated by means of the data collected on an industrial plant for tomato concentrate sterilization. A similar model on the staggered helical fins geometry was previously validated against analytical solution available for the nonfinned annulus for non-Newtonian flows (Pagliarini *et al.*, 2024b). The effect of varying number of finned modules along the length of the HE is investigated at same nominal mass flow rate at the inlet. The results, including heat transfer enhancement, pressure drop augmentation and fluid thermal mixing for different displacements of finned modules, are discussed in relation to the effects induced by the staggered fins through the hydrodynamic and thermal entrance regions of the TTHE. The outcome of the present research provides a useful approach in the design of TTHEs for non-Newtonian fluids processed in the food industry, by fostering optimization strategies able to enhance the overall efficiency of the plant. Hence, the newly proposed augmented geometry may stand as a possible and valuable solution for thermal treatment applications involving highly viscous fluids and, more specifically, food products.

2. Methods

In the present section, the industrial plant is first described in its parts. The mathematical formulation adopted to model tomato processing through the considered sterilizer is therefore presented, and the numerical approach is finally described.

2.1 Industrial plant

The experimental analysis, performed to validate the numerical approach adopted in the present work, is carried out on a sterilizer of an industrial plant for tomato processing. In particular, the system under investigation is a TTHE in a counterflow arrangement, having the hot service fluid flowing through the external annulus and internal tube, whereas the cold process fluid flows through the internal annulus. A section view of the system is shown in Figure 1. For the present application, the process fluid is tomato concentrate (°Bx = 28), while the service fluid is saturated vapor.

The novel feature of the analyzed HE is represented by the presence of stationary finned modules in the internal annulus, whose geometrical features are outlined in Figure 2. They

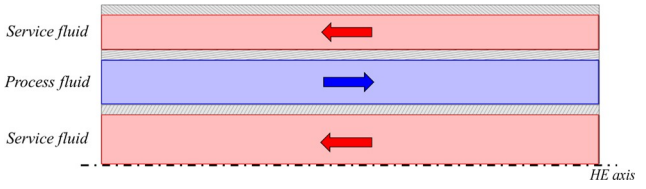

Figure 1. Section view of the system, with reference to the service and process fluids flow direction
Source: Authors' own work

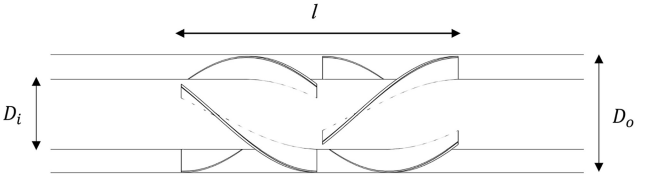

Figure 2. Finned module in the internal annulus of the sterilizer
Source: Authors' own work

are constituted by six twisted fins made of stainless steel, arranged to enhance heat transfer by promoting fluid mixing and boundary layer disruption. The fins in each module are interrupted at the midpoint of the section, and they therefore proceed in a staggered configuration. The ratio between inner and outer diameters is equal to $D_i/D_o = 0.6$, while the length of the finned module is $l = 2.5D_i$.

The sterilizer is made of six straight triple-tube passages of length $L = 24l$, connected by curves having curvilinear length equal to $L_c = 2\,l$. The first passage presents four-finned modules, spaced $d_1 = 6\,l$ apart, while the others present eight-finned modules each, spaced $d_2 = 2\,l$ apart. A drawing of the HE is shown in Figure 3. The inlet and outlet are represented by a blue and a red arrow, respectively. A section view of the first curve is additionally included in the bottom left of Figure 3.

The process fluid temperature and pressure were monitored by means of 2 pressure transducers (Endress Hauser© Cerabar PMP71, full scale = 200, precision 0.05% of full scale, sampling frequency = 1 Hz) and 12 Pt100 (Endress Hauser iTHERM CableLine TST310, tolerance = 0.3°C, sampling frequency = 0.1 Hz), located at three curves as shown in Figure 3. In Figure 4(a), a picture of the instrumented curves is shown. In particular, four Pt100 sensors were placed, at each curved section, at varying penetration lengths into the fluid stream and different circumferential positions. The Pt100 sensors location is depicted in Figure 4(b); the subscripts *S*, *M* and *L* stand for "Short," "Medium" and "Long" penetration length, respectively.

The sensors continuatively acquired signals during plant functioning. In nominal operation, the mass flow rate m of processed tomato concentrate was equal to 1.3 kg/s.

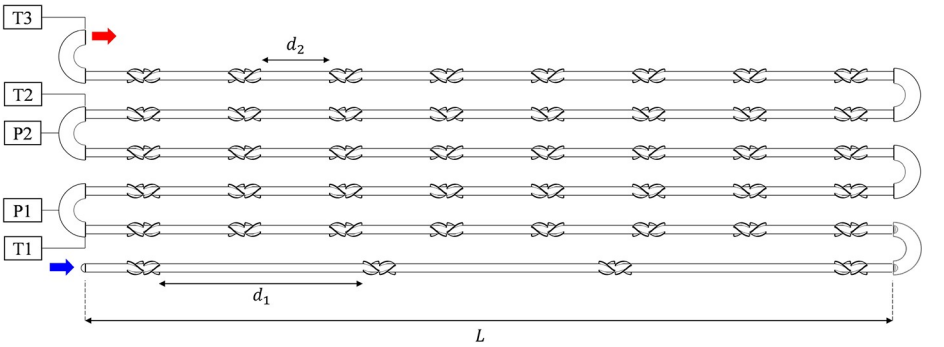

Figure 3. Schematic layout of the sterilizer under investigation
Source: Authors' own work

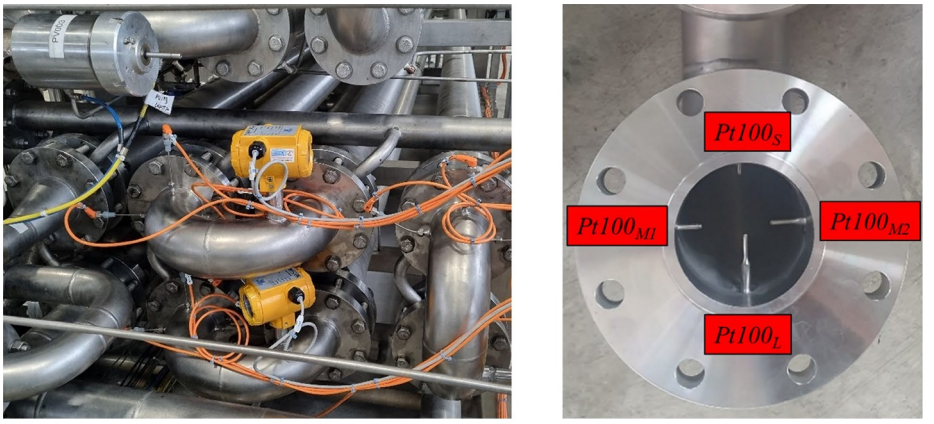

(a) **(b)**

Figure 4. Finned module in the internal annulus of the sterilizer
Source: Authors' own work

2.2 Mathematical formulation

The tomato concentrate flow through the industrial sterilizer under study was modeled by considering the assumptions of incompressible, steady-state, laminar forced flow, with negligible viscous dissipations, constant thermal properties and negligible axial conduction in the fluid. The continuity, momentum and energy equations governing the non-Newtonian, annular flow under investigation are listed below, respectively, in their general formulation for purely viscous fluids (Schlichting and Gersten, 2017):

$$\nabla \cdot \boldsymbol{u} = 0 \tag{1}$$

$$\rho \boldsymbol{u} \cdot \nabla \boldsymbol{u} = -\nabla P + \nabla \cdot \boldsymbol{\tau} \tag{2}$$

$$\boldsymbol{u} \cdot \nabla T = \alpha \nabla^2 T \tag{3}$$

where u is the velocity vector, P is the fluid pressure, $\boldsymbol{\tau}$ is the stress tensor, T is temperature, ρ is the density and α is the thermal diffusivity. To note, equations (1)–(3) can describe the

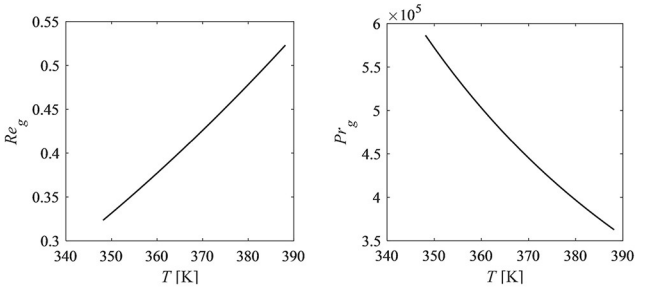

(a) **(b)**

Figure 5. (a) Generalized Reynolds number and (b) Prandtl number in the nominal temperature range of the studied sterilizer
Source: Authors' own work

thermofluid dynamics of either Newtonian or non-Newtonian fluids, depending on the used definition of stress tensor in the momentum equation. Further considerations on how the non-Newtonian stresses are handled in the present work are discussed in the following subsection 2.3. The governing equations are completed, for the present case study, by the following boundary conditions representing uniform axial flow and temperature at the inlet section:

$$u(x, r)_{x=0} = u_{inlet} \tag{4}$$

$$T(x, r)_{x=0} = T_{inlet} \tag{5}$$

$$T(x, r)_{r=D_i/2} = T(x, r)_{r=D_o/2} = T_{wall} \tag{6}$$

where x and r are the axial and radial coordinates, respectively. Hydrodynamic and thermal entrance was accounted for by imposing, at the inlet, uniform velocity and temperature equal to $u_{inlet} = \frac{m}{\rho\pi\left(D_o^2 - D_i^2\right)/4}$ and T_{inlet} = 348.15 K, respectively. Specifically, the inlet temperature reflected the one resulted by nominal operation of the plant upstream the sterilizer. The wall temperature at the inner and outer surfaces of the internal annulus, i.e. at the separation walls between process and service fluid (Figure 1), was kept constant during the process, T_{wall} = 388.15 K. The curves wall was considered as adiabatic.

Conjugate heat transfer at the fluid–solid (fins-to-fluid) interface was considered, ensuring continuity of temperature and heat flux at the boundaries. The interfacial conditions read as:

$$T_s|_\Gamma = T_f|_\Gamma \tag{7}$$

$$k_s \frac{\partial T_s}{\partial \hat{n}}\bigg|_\Gamma = k_f \frac{\partial T_f}{\partial \hat{n}}\bigg|_\Gamma \tag{8}$$

where the subscripts s and f stand for "solid" and "fluid," respectively, Γ is the solid–fluid interface, k is the thermal conductivity and $\hat{n}$ is the unity vector normal to the interfaces.

2.3 Thermal and rheological properties of tomato concentrate

In the numerical analysis, the density, specific heat and thermal conductivity of tomato concentrate were considered equal to ρ = 1,150 kg/m^3, c_p = 3,600 J/kgK and k = 0.5 W/mK, respectively, according to the previous findings by Choi and Okos (1983). The rheological behavior of tomato concentrate was modeled by a power-law model of the form:

$$\eta_a = K|\dot{\boldsymbol{\gamma}}|^{n-1} \tag{9}$$

where η is the apparent viscosity, K is the consistency index, $|\dot{\gamma}|$ is the magnitude of the rate-of-strain tensor and n is the flow behavior index. The latter was considered as constant and equal to 0.15 (Dak *et al.*, 2008). On the contrary, the consistency index was considered to vary with temperature in accordance with the Arrhenius' law:

$$K(T) = Ae^{E_a/RT} \tag{10}$$

where A is a constant, E_a is the activation energy, R is the universal gas constant (8.314 J/molK) and T is the absolute temperature. For the present tomato concentrate, A and E_a were considered equal to 1.93 Pa·s^n and 13,500 J/mol, respectively, according to the previous literature (Dak *et al.*, 2008). Hence, in equation (2), the non-Newtonian stresses are related

with the velocity gradients by the generalized Newtonian model $\boldsymbol{\tau} = \eta_a \boldsymbol{\gamma}$ (Missirlis *et al.*, 2001).

In the light of the considered properties, the tomato concentrate under investigation can be characterized by means of the generalized Reynolds number by Metzner and Reed (1955) and the generalized Prandtl number (Farajzadeh and Tohidi, 2019), respectively, defined as follows:

$$Re_g = \frac{\rho W^{2-n} D_h^n}{8^{n-1} K \left(\frac{3n+1}{4n}\right)^n} \tag{11}$$

$$Pr_g = \frac{c_p K}{k} \left(\frac{W}{D_h}\right)^{n-1} \tag{12}$$

where W is the average velocity and $D_h = D_o - D_i$ is the hydraulic diameter.

Re_g and Pr_g are shown for the nominal temperature range of the studied sterilizer, such as $T_{inlet} \leq T \leq T_{wall}$, in Figure 5(a) and (b), respectively.

The reported data well reflect the extreme working conditions encountered during food processing, and they also suggest an extreme penalization in the heat transfer capabilities. In fact, the high apparent viscosity results in a flow regime regarded as deep laminar, further characterized by a significantly high generalized Prandtl number which hampers thermal penetration into the fluid core. This confirms the extreme need for passive heat transfer enhancement techniques for the present application. It has to be stressed that the low values of generalized Reynolds number reached during the operating conditions under investigation are in line with those considered by the previous literature on thermal treatment of tomato concentrates (Rios-Iribe *et al.*, 2015), where the generalized Reynolds number can often drop below unity.

2.4 Numerical approach

The finite-volume method was applied to discretize and solve the equations for continuity, momentum and energy of subsection 2.2 within an ANSYS© Fluent 2023 R1 environment. To note, the deep laminar nature of the investigated flow prevented the adoption of any transformation or closure equation in the resolution of the governing equations. The computational framework was specifically designed to capture the laminar flow features and heat transfer phenomena within the complex geometry, accounting for the boundary conditions and the non-Newtonian behavior of tomato concentrate. The solid and fluid domains constituting the internal annulus of the HE were meshed using polyhedral elements through the ANSYS© Fluent Mesher 2023 R1, ensuring an accurate representation of the sharp gradients expected at the walls. Seventeen inflation layers were applied at the walls, including the fin surfaces, with a growth rate of 1.1, allowing smooth cell size transition. The adopted grid is shown in Figure 6. It has to be stressed that a high-quality and high-density computational mesh is here required in the light of the low flow behavior index considered in the present investigation, which may hamper proper convergence of the governing equations solution due to the their high nonlinearity (Khandelwal *et al.*, 2015). The SIMPLE (Semi-Implicit Method for Pressure-Linked Equations) algorithm was used for pressure–velocity coupling, as it offers both stability and efficiency in laminar flow simulations. Discretization of the continuity equation is handled by means of the approach proposed by Rhie and Chow (1983) to prevent unphysical pressure fluctuations. Least squares cell-based gradient evaluation is used. For spatial discretization, a second-order upwind scheme was used for the

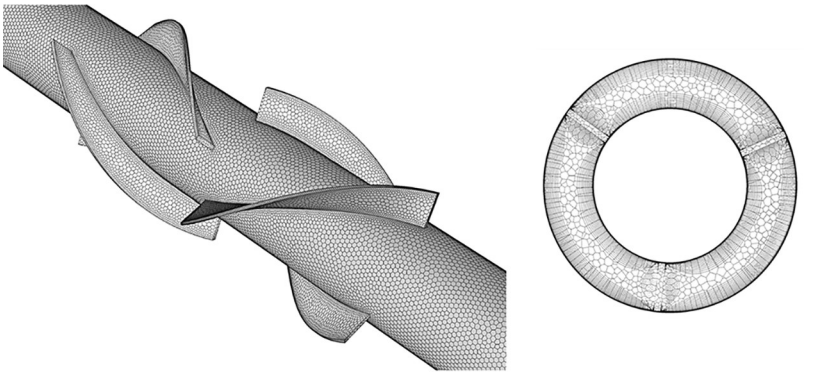

Figure 6. Detail of the adopted mesh
Source: Authors' own work

governing equations to enhance solution accuracy. Default underrelaxation factors are adopted. Before calculations, hybrid initialization algorithm is performed. The absolute convergence criterion for all the residuals was set to 1E-6.

The simulated configurations are listed in Table 1. All the simulations were run under the same boundary and test conditions defined in subsection 2.2.

3. Uncertainty analysis

The uncertainties related to the collected experimental quantities were assessed to understand the robustness of the present study approach. Specifically, the uncertainty related to the fluid pressure drops resulted from considerations related to the employment of two absolute pressure transducers, as previously highlighted in Figure 3. Hence, the uncertainty $\delta P_{differential}$ to be attributed to the pressure drop between the P1 and P2 locations read as $\delta P_{differential} = \sqrt{2 \cdot \delta P_{absolute}^2}$, where $\delta P_{absolute}$ is the uncertainty referred to the single pressure transducer. For the adopted equipment, $\delta P_{differential}$ was computed equal to 0.14 bar.

For what concerns fluid temperature acquisitions, provided that the temperature at the locations T1, T2 and T3 (according to Figure 3) is evaluated as the average between the

Table 1. Simulated geometrical conditions

Simulations	Simulated geometry	Aim
1	Single-finned module (Figure 2)	Grid independence analysis
2	Sterilizer (Figure 3)	Experimental validation
3	First triple-tube annular passage + curve; four-finned modules	Evaluating the thermal enhancement of different configurations with respect to the reference geometry (nonfinned)
4	First triple-tube annular passage + curve; eight-finned modules	
5	First triple-tube annular passage + curve; nonfinned	

Source(s): Authors' own work

signals acquired by the four pt100 sensors at each monitored section, the uncertainty of mean section temperatures is considered as the uncertainty of the single temperature measurement, i.e. 0.3°C. Such a conservative uncertainty choice is driven by the fact that the measured temperature at different fluid positions in the generic tube section is highly variable.

4. Grid independence

Grid independence analysis was performed to ensure the reliability of the numerical results by considering a single-finned module of length l. The geometrical characteristics of the adopted grid were progressively refined, as reported in Table 2, until the chosen quantities, namely, the Nusselt number and the friction factor, stabilized.

All the grids presented an orthogonal quality higher than 0.3. For grid independence analysis, the friction factor f and the Nusselt number Nu were chosen as meaningful quantities to be monitored. Their definitions are reported below:

$$f = \Delta P_{x \to x+\Delta x} D_h / \left(2\rho W^2 \Delta x\right) \tag{13}$$

$$Nu = \frac{hD_h}{k} \tag{14}$$

where $\Delta P_{x \to x+\Delta x}$ is the pressure drop between two consecutive axial coordinates x and $x + \Delta x$, h is the convective heat transfer coefficient and k is the fluid thermal conductivity. For the present case of imposed temperature at the inner/outer surfaces of the annulus, h was estimated, for each annulus section of length Δx, by means of the following expression:

$$h = \frac{Q}{A_{tot} * \Delta T_{ml}} = \frac{\dot{m} c_p (T_{b,out} - T_{b,in})}{A_{tot} * \Delta T_{lm}} \tag{15}$$

where Q is the thermal power exchanged, A_{tot} is the total heat transfer area, $T_{b,in}$ and $T_{b,out}$ are the bulk temperatures at the inlet and outlet, respectively, of the considered annulus section, while ΔT_{lm} is the logarithmic mean temperature difference, defined as:

$$\Delta T_{lm} = \frac{(T_{wall} - T_{b,in}) - (T_{wall} - T_{b,out})}{\log\left(\frac{T_{wall} - T_{b,in}}{T_{wall} - T_{b,out}}\right)} \tag{16}$$

In Figure 7(a)–(b), Nu and f are plotted against the number of elements. Because both quantities stabilized for grids having about 3 million elements, the geometrical features of grid C were used for the present study. Such a choice allows a good trade-off between accuracy of the results and needed computational cost.

Table 2. Characteristics of the adopted grids for the single-finned module

Grid	A	B	C	D	E
Minimum size [m]	0.002	0.0017	0.0012	0.0008	0.00065
Maximum size [m]	0.006	0.005	0.0037	0.0022	0.00135
Inflation layers	10	15	15	17	20
Number of elements	4.49E + 05	8.27E + 05	1.46E + 06	2.99E + 06	6.90E + 06

Source(s): Authors' own work

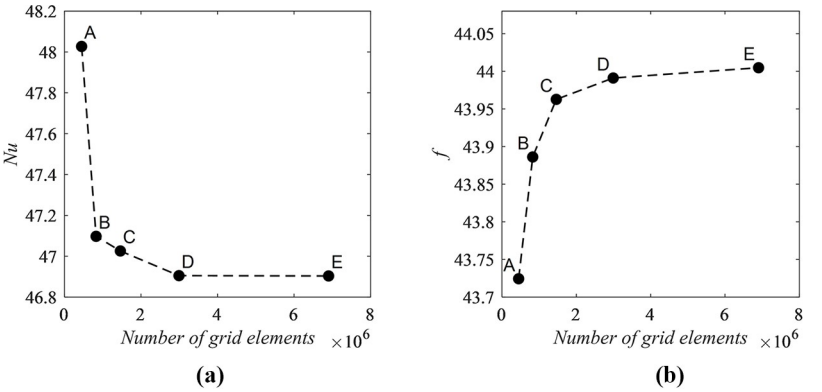

(a) (b)

Figure 7. Grid independence analysis
Source: Authors' own work

5. Results

Experimental results are first presented to underline temperature evolution and pressure drops in the real system. Reduced experimental data are therefore adopted to thoroughly validate the numerical method. Finally, numerical results are adopted to better understand the flow features characterizing the proposed solution, as well as its impact on the heat transfer augmentation features, frictional losses and overall thermal mixing.

5.1 Experimental data

In the present section, the experimental data collected during in-situ monitoring of the tomato concentrate processing plant is presented. In Figure 8, the temperature signals, acquired at the three locations T1, T2 and T3, according to Figure 3 over the observation window, are shown. To note, the temperature is here expressed in dimensionless form $\theta = T/T_{wall}$. At the first acquisition point [Figure 8(a)], the temperatures referred to the sensors having medium and long penetration lengths are close to the inlet temperature, $\theta_{inlet} = T_{inlet}/T_{wall} = 0.65$, suggesting that the fluid core is still at much lower temperature than the wall. On the contrary, the fluid close to the wall is already significantly warmed up, as

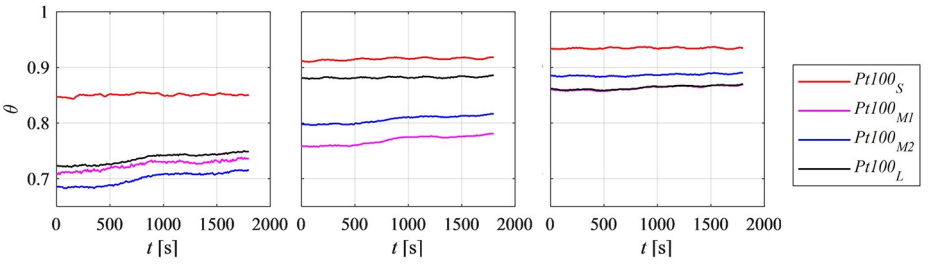

(a) (b) (c)

Figure 8. Pt100 sensors signals over time referred to the (a) T1, (b) T2 and (c) T3 locations, according to Figure 3
Source: Authors' own work

confirmed by the sensor having short penetration length (red solid line). At the second acquisition point [Figure 8(b)], all the temperature data exhibit a noticeable increase. The beneficial effects of the finned modules on the overall mixing and thermalization of the process fluid is perceivable by the fact that the sensor having long penetration length (black solid line) approaches here the one having short penetration length, suggesting that the fluid recirculation promoted by fins successfully forces the fluid in contact with the heating walls to flow closer to the core of the annular passage. Thanks to such a recirculation effect, overheating of tomato concentrate is mitigated, whereas colder fluid could be effectively redirected toward the heating walls, allowing better efficiency of the sterilization process. Finally, at the last acquisition point [Figure 8(c)], the fluid temperature at the four sensors locations exhibits good homogenization, being the recorded signals close to each other. Such evidence confirms the capability of the finned modules to enhance fluid mixing and, consequently, its thermalization during the sterilization process. From the experimental temperature signals provided, the temperature stratification characterizing the fluid flow during thermal treatment is evident, especially closer to the HE inlet. Such a critical issue will be numerically dealt with by analyzing the effect of different geometrical configurations on heat transfer augmentation in subsection 5.3.

The gauge pressure signals, synchronized with the temperature signals of Figure 8, were also reduced to evaluate the pressure drop along the HE. In Figure 9, the pressure drops per unit length between the first and the second pressure measurement locations, ΔP = P1 – P2, are shown, being $L_P = 2L + 2L_c$, according to Figure 3. The high viscosity of processed tomato concentrate results in high pressure losses, further increased by the presence of the finned modules. Despite the intrinsic noise of the signal, the pressure drops exhibit a slight variation over time, which is probably due to small deviations of the plant from its nominal conditions of mass flow rate at the inlet of the sterilizer during functioning.

By adopting experimental pressure data, the assumption drawn in subsection 2.2 for negligible viscous dissipation was verified. Specifically, such an assumption holds when the Brinkman number is limited (Gratão *et al.*, 2006). When a non-Newtonian flow in

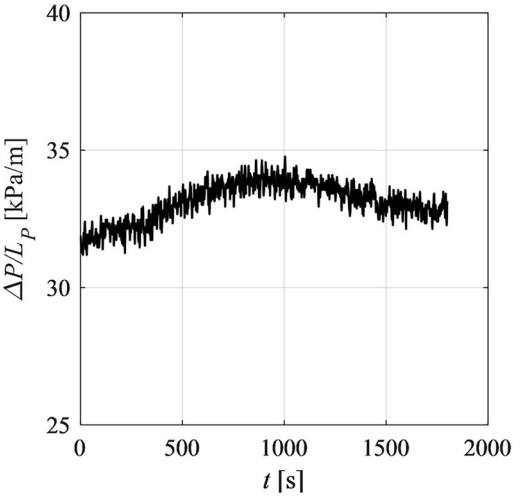

Figure 9. Pressure drops per unit length between P1 and P2 (reference of Figure 3) over time
Source: Authors' own work

developed, constant wall temperature conditions is considered, the Brinkman number assumes the generalized form below (Coelho and Pinho, 2009):

$$Br_g = \frac{W\tau_{wall}D_h}{8k(T_{wall} - T_{inlet})} \tag{17}$$

where the wall shear stress can be defined as a function of the friction factor, $\tau_{wall} = \frac{fW^2\rho}{8}$. By assuming the flow fully developed between the two pressure locations P1 and P2, and by estimating f through the recorded $\Delta P/L_P$ (Figure 9), Br_g results lower than 10^{-2}, hence confirming the negligible viscous dissipations in the fluid flow.

5.2 Validation of the numerical approach

The numerical approach has been validated by means of the data experimentally acquired on the analyzed industrial plant. Specifically, all the experimental samples were averaged over the observation window. The same locations of the sensors experimentally used were considered for the extraction of numerical results. Specifically, temperature and pressure data were exported by performing surface averages at the sections of interest. In Table 3, numerical and experimental temperature and pressure data are listed. Percentage deviations between numerical (dat_{num}) and experimental ($dat_{\exp}$) data were additionally computed as $PD = \frac{dat_{num} - dat_{\exp}}{dat_{\exp}} \times 100$, and reported.

As noticeable, the percentage deviations between numerical and experimental data are limited, suggesting a very good agreement between the adopted pieces of data and, consequently, a high reliability of the used numerical approach. To provide an additional piece of validation of the numerical scheme, the average dimensionless temperature assumed by the simulated flow along the heat exchanger is plotted in Figure 10, together with the experimental data for comparison. Here, it is noticeable that the temperature trend along the dimensionless axial coordinate is coherent with the imposed heating conditions. The model is further confirmed to well approximate the temperature evolution in the real experimental system, discretized at the monitoring sections. The numerical method was thus considered as fully validated because it reflected with good accuracy the values of pressure drops and dimensionless temperatures recorded during the industrial plant operation.

5.3 Numerical results

After successfully validating the numerical method against experimental data, the main thermofluid dynamics features promoted by the finned modules were numerically investigated. To note, all the simulations were carried out by considering mass flow rate of 1.3 kg/s, such as the same mass flow rate treated by the industrial plant during nominal operation. First, a local analysis of the results allowed a better representation of the flow and

Table 3. Comparison between numerical and experimental data

Variable	Numerical data	Experimental data	PD (%)
ΔP (kPa/m)	31.05	32.13	3.4
θ_1	0.78	0.75	4.0
θ_2	0.84	0.84	0
θ_3	0.89	0.87	2.3

Source(s): Authors' own work

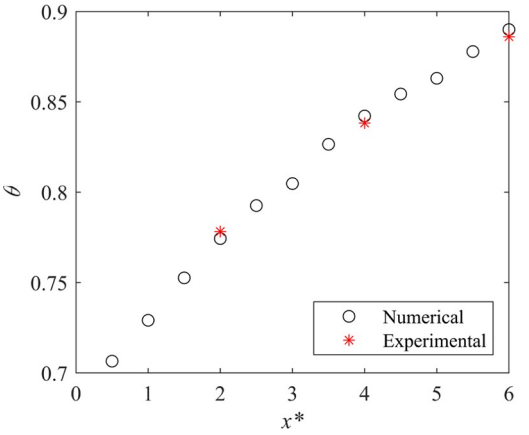

Figure 10. Comparison between numerical and experimental average dimensionless fluid temperatures along the dimensionless axial coordinate of the HE
Source: Authors' own work

thermal characteristics through finned geometries. The effectiveness of the proposed solution was therefore analyzed in terms of heat transfer augmentation and fluid thermalization with respect to the reference geometry, such as the nonfinned annulus under same operating conditions. Geometrical arrangements presenting four- and eight-finned modules, respectively, were investigated during the thermal and hydrodynamic entrance region, i.e. in the first triple-tube passage, and compared to identify the optimal configuration from a thermofluidic standpoint.

5.3.1 Local flow and thermal characteristics. The finned geometry of the HE was first analyzed in terms of local features of the fluid flow. Streamlines are shown in Figure 11(a) for a representative finned module. As noticeable, the finned geometry induces significant variations of the fluid path: the fluid crosses the first part of the module, undergoing swirling effects which are believed to augment the heat transfer capabilities of the system (Mousavi Ajarostaghi *et al.*, 2022). Moreover, the middle section of the module ensures a drastic change in fluid flow direction, probably allowing better fluid mixing and overall thermalization. In Figure 11(b), velocity contours are shown along the finned module. Here, it can be noted that the velocity contours at the two ends of the module reflect the ones expected for an unperturbed annular flow, being the velocity in the core of the annulus highly uniform.

Close to the finned module, the fins effect becomes more and more evident. The fluid is circumferentially accelerated, being forced to follow the fins paths. In the middle of the finned sections, i.e. at the fins' interruption and consequent path inversion, high nonuniformity of fluid velocity occurs. Such an interruption is in fact expected to greatly enhance heat transfer, according to previous studies on interrupted fins (El Maakoul *et al.*, 2020; Mohsen *et al.*, 2021).

In Figure 12, the dimensionless temperature contours along a representative module are shown. Here, the temperature referred to the fluid in contact with the heating walls is much higher than that in the core of the annulus. This confirms the fact that the high Prandtl characterizing the investigated flow prevents heat diffusion into the fluid core, penalizing its proper thermalization. Nonetheless, the temperature contours through the finned module exhibit the presence of warm spots away from the inner and outer walls, probably due to the joint effect

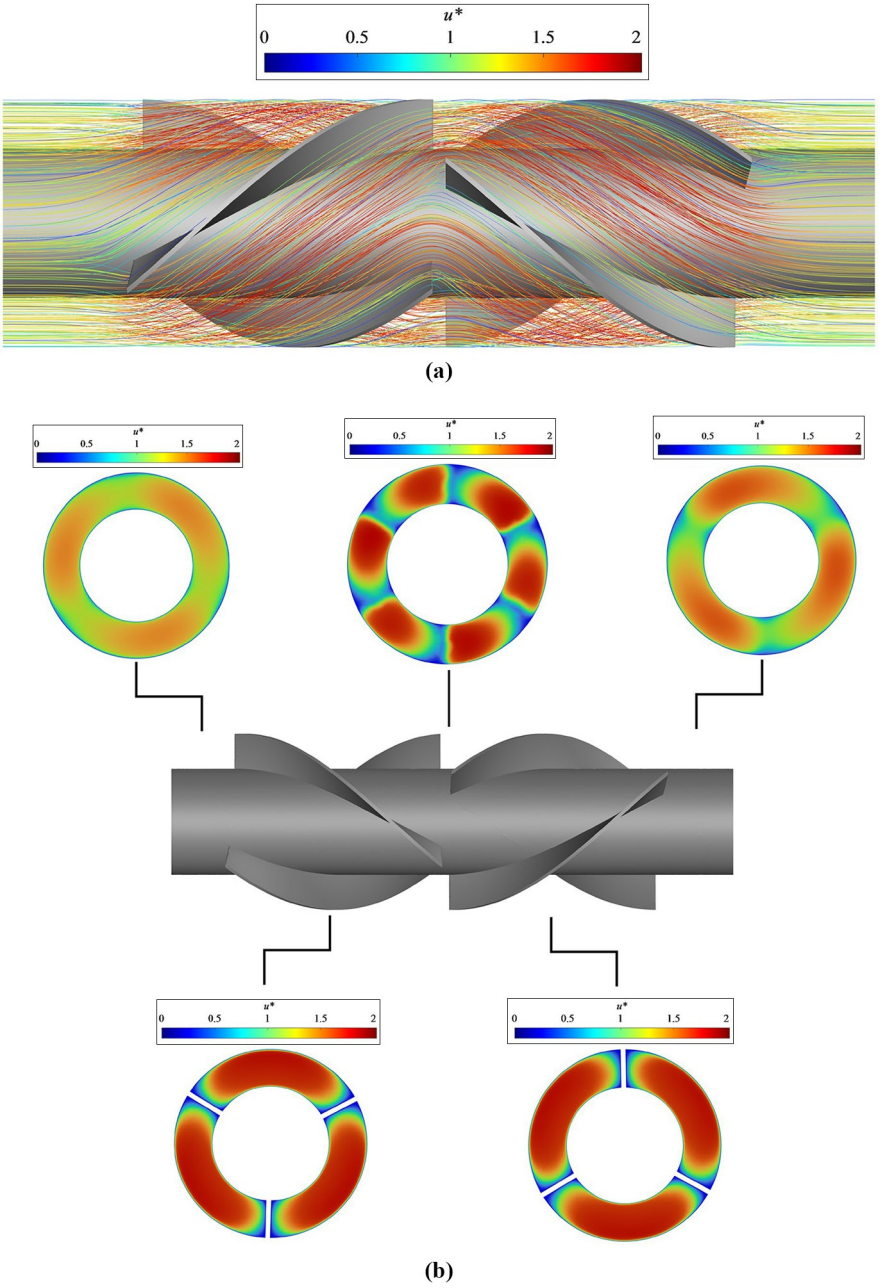

Figure 11. (a) Streamlines and (b) dimensionless velocity contours along a representative finned module of the studied HE

Source: Authors' own work

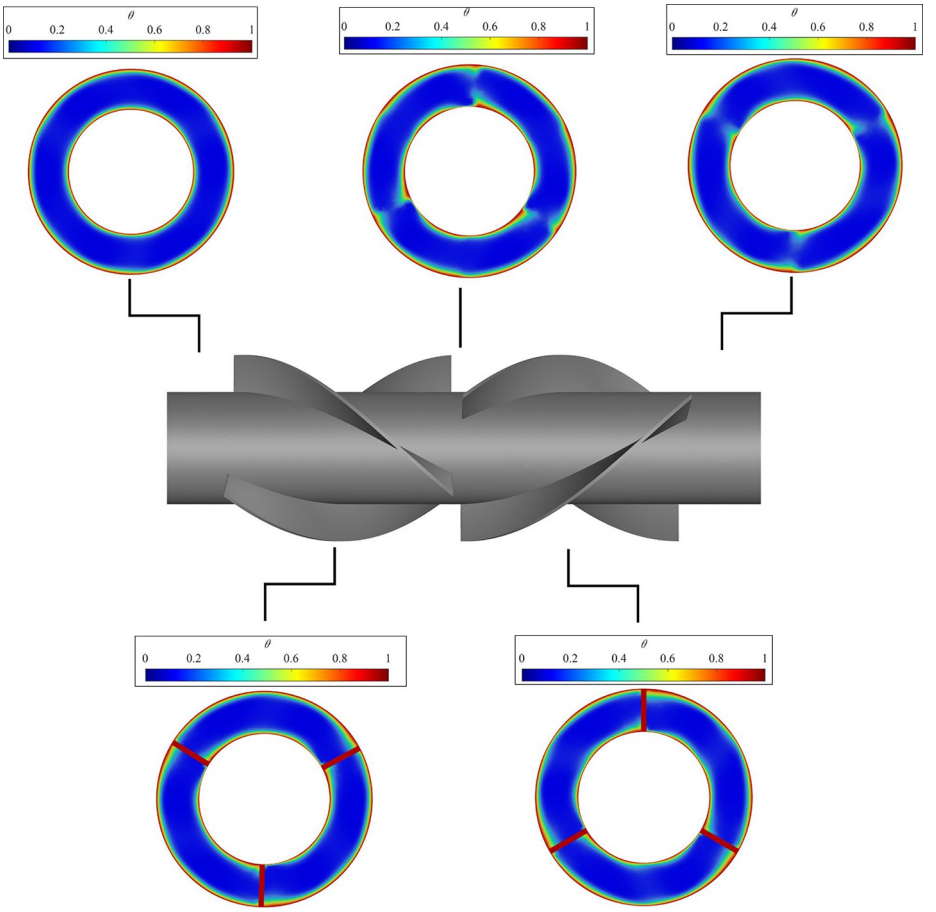

Figure 12. Dimensionless temperature contours along a representative finned module of the studied HE
Source: Authors' own work

of enhanced inner convection promoted by the fins and heat transfer through the fins. The latter is, however, believed to play a minor role in the overall heat transfer processes due to low thermal conductivity of stainless steel. Finally, downstream the fins, the warm spots in the fluid tend to progressively disappear, probably due to inner conduction in the fluid core.

5.3.2 Heat transfer enhancement. After achieving a better local description of the thermofluid dynamics characterizing the finned solution, the heat transfer efficiency of the finned HE was quantified by estimating the Nusselt number and the friction factor along the entrance region of the HE, such as from the inlet of the sterilizer up to the end of the first curve. In particular, the study on the hydrodynamic and thermal entrance region of the system is of practical importance to design compact HEs (Batra and Sudarsan, 1992).

In Figure 13, the Nusselt number for the finned (eight and four modules) and nonfinned configurations is shown against the dimensionless axial coordinate, defined as $x^* = x/L$.

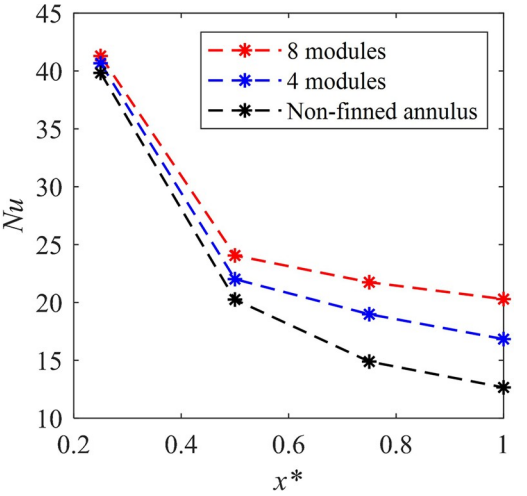

Figure 13. Nusselt number as a function of the dimensionless axial coordinate
Source: Authors' own work

For $x^* = 0.25$, all configurations show similar Nusselt numbers, suggesting that the first thermal entrance is not significantly affected by fins. At increasing dimensionless axial coordinate, both the finned geometries present higher *Nu* with respect to the nonfinned configuration, highlighting the efficacy of fins in terms of passive heat transfer enhancement. The provided values of *Nu* in the enhanced configuration are in line with those typically found for similar applications adopting scraped surface HEs (Solano *et al.*, 2023; Triki *et al.*, 2021), denoting comparable heat transfer augmentation at the cost of obvious higher energy consumption than the proposed finned solution. Nonetheless, the configuration with eight-finned modules exhibits the highest thermal performance as long as the flow develops (*Nu* almost twice the one of the nonfinned geometry at $x^* = 1$). This is due to the greater flow perturbance achieved by the higher number of finned modules, which establishes a more effective boundary layer disruption. The effect of different numbers of finned modules on the friction factor is further reported in Figure 14.

As expected, for the same test conditions, the presence of more finned modules results in higher friction factors, whereas the nonfinned geometry exhibits the lowest friction factor. The computed values of friction factor are in agreement with those expected for non-Newtonian flows under laminar conditions, as reported in Madlener *et al.* (2009).

In the light of the presented figures of merit, the configuration having eight-finned modules highlights better thermal performances, at the cost of higher friction factor according to the well-established analogy between heat and momentum transfer (Mahulikar and Herwig, 2008). To quantify the effect of pressure drops over heat transfer enhancement of the two configurations, the performance index η was computed for both the finned geometries as (Gomaa *et al.*, 2017):

$$\eta = \frac{Nu/Nu_0}{f/f_0} \tag{18}$$

where the subscript 0 refers to the reference geometry (nonfinned annulus). η is plotted against the dimensionless axial coordinate in Figure 15. Here, η is less than unity for the first

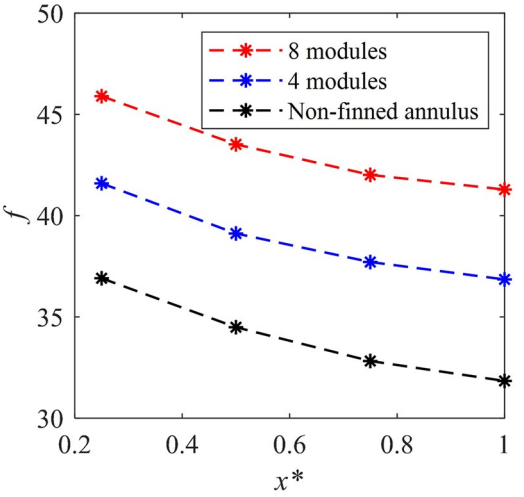

Figure 14. Friction factor as a function of the dimensionless axial coordinate
Source: Authors' own work

length of the entrance length, i.e. $x^* < 0.6$, confirming that the presence of fins does not play any beneficial role at the beginning of the entrance region. This could be due to the considered high Prandtl number, for which the hydrodynamic boundary layer develops much faster than the thermal boundary layer (Batra and Sudarsan, 1992).

However, for $x^* > 0.7$, η becomes greater than unity, suggesting better thermofluidic performances of the internal annulus presenting fins. Specifically, the use of four-finned

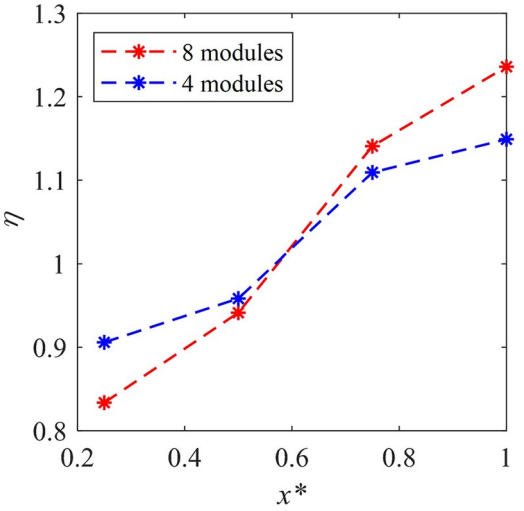

Figure 15. Performance index η estimated for the eight- and four-finned modules
Source: Authors' own work

modules results in a maximum η of about 1.15, while the annulus presenting eight-finned modules exhibits the highest η in the entrance region (maximum of about 1.23 at $x^* = 1$). Such a configuration is hence confirmed to be superior in terms of heat transfer augmentation, despite the increased pressure losses.

5.3.3 Thermal mixing. The analysis on overall heat transfer augmentation achieved through the present passive, finned solutions were completed by the evaluation of their thermal mixing efficiency. This is, in fact, a fundamental parameter to ensure proper thermal processing of the food product without degrading its chemical and functional properties (Sawale *et al.*, 2024; Sikorski, 2006). Hence, the effectiveness of the proposed finned modules in terms of thermalization of the process fluid was investigated by estimating a thermal mixing parameter ψ, defined as follows (Kouadri *et al.*, 2021):

$$\psi_i = 1 - \frac{\sigma_i}{\sigma_{i,0}} \tag{19}$$

where σ_i and $\sigma_{i,0}$ are the temperature standard deviation in the generic cross section i related to the finned configuration, and the temperature standard deviation evaluated at the same section for the reference, nonfinned geometry. To note, when the temperature standard deviation in the finned annulus equals the one in the nonfinned annulus, $\psi = 0$ (minimum mixing improvement achievable), whereas $\psi = 1$ when the temperature standard deviation of the finned annulus equals zero (maximum mixing improvement achievable).

In Figure 16, ψ is shown as a function of the dimensionless axial coordinate. Here, the thermal mixing parameter is always greater than zero, and it keeps increasing along the axial coordinate for every configuration, suggesting that the presence of fins can effectively increase the fluid thermalization with respect to the nonfinned configuration. The geometry presenting eight-finned modules always exhibits higher values of ψ, with a maximum of 0.11, suggesting not only greater heat transfer, as per subsection 5.3.2, but also higher thermal mixing of the working fluid, thus proving its superior thermal performance.

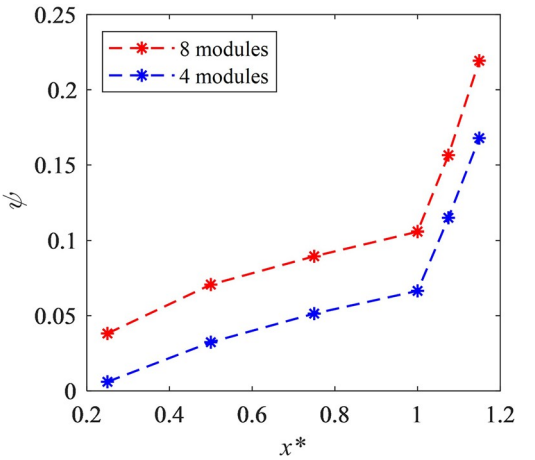

Figure 16. Mixing parameter as a function of the dimensionless axial coordinate
Source: Authors' own work

It is worth noticing that, for $x^* > 1$, i.e. in the curve, ψ undergoes a sharp increase, hence suggesting that, despite the curved connections are considered as adiabatic, their effect on the fluid thermal mixing is extremely beneficial. To provide a better insight into such increased thermal mixing, a dimensionless temperature contour of the curve section is shown in Figure 17. When the heating section interrupts, the fluid expands in the curve, and the threads close to the hot, inner wall proceed along the core of the curved section. This results in the formation of a hot fluid trail, continuously warmed up by the ending tip of the inner tube of the HE. Hence, despite the inner convection does not substantially increase due to low accelerations induced by curvature, the fluid experiences higher thermal mixing due to section variation and continuous warming up of the fluid core.

6. Conclusions

A TTHE for tomato concentrate sterilization was experimentally and numerically tested via CFD to assess heat transfer enhancement achievable by interrupted, staggered fins in the internal annulus. The industrial plant was instrumented with pressure and temperature transducers at varying locations to monitor the main characteristics of the tomato concentrate thermal processing. The governing equations and corresponding boundary conditions were implemented in an ANSYS© Fluent environment. The rheological behavior of tomato concentrate was modeled by means of a power-law model, with consistency coefficient dependent on temperature. After a grid independence analysis on a

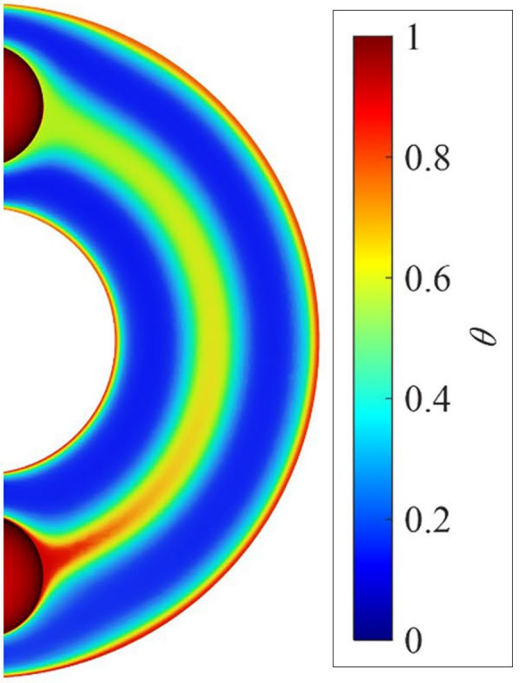

Figure 17. Temperature contour referred to the curve section
Source: Authors' own work

single-finned module, the geometrical features of the optimal grid were used to simulate the entire sterilizer. The numerical data were compared with experimental ones to achieve a proper validation of the numerical approach. The maximum deviation between experimental and numerical data was equal to 4%. The features of the considered flow through a representative finned module were locally investigated by means of dimensionless velocity and temperature contours. Different geometrical configurations, i.e. finned system with eight-finned modules, finned system with four-finned modules and nonfinned annulus, were therefore simulated in the entrance region to assess the heat transfer augmentation promoted by fins. The Nusselt number *N*u and the friction factor *f* were assessed as functions of the dimensionless axial coordinate. The geometry having superior thermal performances and, at the same time, introducing limited pressure losses was selected by means of the performance index η. The thermal mixing achieved by fins was finally evaluated through a thermal mixing parameter ψ.

The following main outcomes can be drawn:

- The presence of fins induces a swirling flow, capable of enhancing heat transfer. Moreover, the staggered configuration promotes better fluid mixing due to higher perturbation of the fluid stream.
- In the entrance region, the annulus having eight-finned modules present the highest *N*u (almost twice the one of the nonfinned geometry), despite the highest friction factor.
- The performance index η for the eight-finned modules reaches a maximum of about 1.23, while the use of four-finned modules guarantees a η of about 1.15. The use of closer finned modules is thus confirmed to be beneficial in terms of overall heat transfer performances of the HE under the operating conditions investigated.
- The fluid thermal mixing resulting from the finned configurations is always greater than zero, suggesting that fins not only promote heat transfer but also fluid thermalization. Up to the curved section, the ψ reaches a maximum of about 0.11 for the geometry presenting eight-finned modules. However, in the curve, ψ undergoes a much steeper increase, reaching a maximum of about 0.22. Such behavior could account for the change in the tube cross section, coupled with trailing thermal effects resulting from the upstream heating section.

To conclude, the adopted finned geometries presented superior performances than the nonfinned annulus due to their boundary layer disruption and thermal mixing effects. Having more frequent finned modules along the HE, i.e. shorter distance between modules, promoted heat transfer enhancement, whereas guaranteeing limited pressure losses. The present study can be used to design more efficient HEs for food processing, especially when good thermal mixing and consequent uniform treatment are required. In fact, this represents a critical aspect in the food industry, where strict temperature targets are needed to achieve a satisfactory degree of microbial and enzyme inactivation and organoleptic characteristics preservation, hence underlining the extreme relevancy of the proposed heat transfer enhancement method for such industrial applications.

In future works, the finned module will be optimized by varying its geometrical features, such as the twist rate. Also, the reported flow and thermal patterns taking place in the curve could be considered to develop novel passive methodologies for maximizing fluid mixing and thermalization at such locations.

Acknowledgments

The Authors would like to acknowledge financial support from PNRR-M4C2- I1.1 – MUR Call for proposals n.104 of 02-02-2022 - PRIN 2022 - ERC sector PE8- Project title: MOOD4HEX - MOr-phology Optimized Design for HEs - Project Code 2022SJP2A5 - CUP Code D53D23004040006 - Funded by the European Union – NextGenerationEU and and from the CFT Group, Parma, Italy (www.cftroup.com/it/).

Data availability

All data underlying the results are available as part of the article and no additional source data are required.

References

Abbasian Arani, A.A. and Moradi, R. (2021), "Shell and tube heat exchanger thermal-hydraulic analysis equipped with baffles and corrugated tubes filled with non-Newtonian two-phase nanofluid", *International Journal of Numerical Methods for Heat and Fluid Flow*, Vol. 31 No. 4, pp. 1214-1244, doi: 10.1108/HFF-04-2020-0186.

Akgul, D., Mercan, H., Acikgoz, O. and Dalkilic, A.S. (2023), "Advances in triple tube heat exchangers regarding heat transfer characteristics of single and two-phase flows in comparison to double tube heat exchangers part 1", *Kerntechnik*, Vol. 88 No. 6, pp. 642-655, doi: 10.1515/kern-2023-0023.

Aytaç, İ., Badali, Y. and Tuncer, A.D. (2023), "Numerical and experimental investigation for enhancing thermal performance of a concentric heat exchanger using different scenarios", *International Journal of Numerical Methods for Heat and Fluid Flow*, Vol. 33 No. 6, pp. 2100-2127, doi: 10.1108/HFF-10-2022-0588.

Bahiraei, M., Mazaheri, N. and Rizehvandi, A. (2019), "Application of a hybrid nanofluid containing graphene nanoplatelet–platinum composite powder in a triple-tube heat exchanger equipped with inserted ribs", *Applied Thermal Engineering*, Vol. 149, pp. 588-601, doi: 10.1016/j.applthermaleng.2018.12.072.

Bahiraei, M., Mazaheri, N. and Hanooni, M. (2021a), "Performance enhancement of a triple-tube heat exchanger through heat transfer intensification using novel crimped-spiral ribs and nanofluid: a two-phase analysis", *Chemical Engineering and Processing – Process Intensification*, Vol. 160, p. 108289, doi: 10.1016/j.cep.2020.108289.

Bahiraei, M., Foong, L.K., Hosseini, S. and Mazaheri, N. (2021b), "Predicting heat transfer rate of a ribbed triple-tube heat exchanger working with nanofluid using neural network enhanced by advanced optimization algorithms", *Powder Technology*, Vol. 381, pp. 459-476, doi: 10.1016/j.powtec.2020.12.003.

Batra, R.L. and Sudarsan, V.R. (1992), "Laminar flow heat transfer in the entrance region of concentric annuli for power law fluids", *Computer Methods in Applied Mechanics and Engineering*, Vol. 95 No. 1, pp. 1-16, doi: 10.1016/0045-7825(92)90078-X.

Bhattacharyya, S., Vishwakarma, D.K., Srinivasan, A., Soni, M.K., Goel, V., Sharifpur, M., Ahmadi, M.H., Issakhov, A. and Meyer, J. (2022), "Thermal performance enhancement in heat exchangers using active and passive techniques: a detailed review", *Journal of Thermal Analysis and Calorimetry*, Vol. 147 No. 17, pp. 9229-9281, doi: 10.1007/s10973-021-11168-5.

Bozzoli, F., Cattani, L. and Rainieri, S. (2020), "Cross-helix corrugation: the optimal geometry for effective food thermal processing", *International Journal of Heat and Mass Transfer*, Vol. 147, p. 118874, doi: 10.1016/j.ijheatmasstransfer.2019.118874.

Bozzoli, F., Cattani, L., Mocerino, A., Rainieri, S., Tougri, I. and Colaço, M.J. (2021), "Characterisation of the heat transfer in displaced enhancement devices by means of inverse problem approach

applied to IR images", *Quantitative InfraRed Thermography Journal*, Vol. 18 No. 2, pp. 108-126, doi: 10.1080/17686733.2019.1700696.

Chakka, A.K., Sriraksha, M.S. and Ravishankar, C.N. (2021), "Sustainability of emerging green non-thermal technologies in the food industry with food safety perspective: a review", *LWT*, Vol. 151, p. 112140, doi: 10.1016/j.lwt.2021.112140.

Choi, Y. and Okos, M. (1983), "The thermal properties of tomato juice concentrates", *Transactions of the ASABE*, Vol. 26, pp. 305-311.

Coelho, P.M. and Pinho, F.T. (2009), "A generalized Brinkman number for non-Newtonian duct flows", *Journal of Non-Newtonian Fluid Mechanics*, Vol. 156 No. 3, pp. 202-206, doi: 10.1016/j.jnnfm.2008.07.001.

Dak, M., Verma, R.C. and Jaaffrey, S.N.A. (2008), "Rheological properties of tomato concentrate", *International Journal of Food Engineering*, Vol. 4 No. 7, doi: 10.2202/1556-3758.1470.

El Maakoul, A., Feddi, K., Saadeddine, S., Ben Abdellah, A. and El Metoui, M. (2020), "Performance enhancement of finned annulus using surface interruptions in double-pipe heat exchangers", *Energy Conversion and Management*, Vol. 210, p. 112710, doi: 10.1016/j.enconman.2020.112710.

Farajzadeh, M.A. and Tohidi, A. (2019), "Mixing and heat transfer enhancement of power-law fluids inside helically coiled tube by chaotic advection", *Journal of Non-Newtonian Fluid Mechanics*, Vol. 274, p. 104202, doi: 10.1016/j.jnnfm.2019.104202.

García-Valladares, O. (2004), "Numerical simulation of triple concentric-tube heat exchangers", *International Journal of Thermal Sciences*, Vol. 43 No. 10, pp. 979-991, doi: 10.1016/j.ijthermalsci.2004.02.006.

Gomaa, A., Halim, M.A. and Elsaid, A.M. (2017), "Enhancement of cooling characteristics and optimization of a triple concentric-tube heat exchanger with inserted ribs", *International Journal of Thermal Sciences*, Vol. 120, pp. 106-120, doi: 10.1016/j.ijthermalsci.2017.06.002.

Gratão, A.C.A., Silveira, V. and Telis-Romero, J. (2006), "Laminar forced convection to a pseudoplastic fluid food in circular and annular ducts", *International Communications in Heat and Mass Transfer*, Vol. 33 No. 4, pp. 451-457, doi: 10.1016/j.icheatmasstransfer.2006.01.006.

Khandelwal, V., Dhiman, A. and Baranyi, L. (2015), "Laminar flow of non-Newtonian shear-thinning fluids in a T-channel", *Computers and Fluids*, Vol. 108, pp. 79-91, doi: 10.1016/j.compfluid.2014.11.030.

Kouadri, A., Douroum, E., Lasbet, Y., Naas, T.T., Khelladi, S. and Makhlouf, M. (2021), "Comparative study of mixing behaviors using non-Newtonian fluid flows in passive micromixers", *International Journal of Mechanical Sciences*, Vol. 201, p. 106472, doi: 10.1016/j.ijmecsci.2021.106472.

Kubo, M.T.K., Baicu, A., Erdogdu, F., Poças, M.F., Silva, C.L.M., Simpson, R., Vitali, A.A. and Augusto, P.E. (2023), "Thermal processing of food: challenges, innovations and opportunities: a position paper", *Food Reviews International*, *Taylor and Francis*, Vol. 39 No. 6, pp. 3344-3369, doi: 10.1080/87559129.2021.2012789.

Madlener, K., Frey, B. and Ciezki, H.K. (2009), "Generalized Reynolds number for non-Newtonian fluids", *EUCASS Proceedings Series – Advances in AeroSpace Sciences*, Vol. 1, pp. 237-250.

Mahulikar, S.P. and Herwig, H. (2008), "Fluid friction in incompressible laminar convection: Reynolds' analogy revisited for variable fluid properties", *The European Physical Journal B*, Vol. 62 No. 1, pp. 77-86, doi: 10.1140/epjb/e2008-00115-0.

Malavasi, M., Cattani, L., Vocale, P., Bozzoli, F. and Rainieri, S. (2021), "Thermal characterisation of triple tube heat exchangers by parameter estimation approach", *International Journal of Heat and Mass Transfer*, Vol. 178, p. 121598, doi: 10.1016/j.ijheatmasstransfer.2021.121598.

Metzner, A.B. and Reed, J.C. (1955), "Flow of non-Newtonian fluids—correlation of the laminar, transition, and turbulent-flow regions", *AIChE Journal*, Vol. 1 No. 4, pp. 434-440, doi: 10.1002/aic.690010409.

Missirlis, K.A., Assimacopoulos, D., Mitsoulis, E. and Chhabra, R.P. (2001), "Wall effects for motion of spheres in power-law fluids", *Journal of Non-Newtonian Fluid Mechanics*, Vol. 96 No. 3, pp. 459-471, doi: 10.1016/S0377-0257(00)00189-0.

Mohsen, O.A., Muhammed, M.A.R. and Hasan, B.O. (2021), "Heat transfer enhancement in a double pipe heat exchanger using different fin geometries in turbulent flow", *Iranian Journal of Science and Technology, Transactions of Mechanical Engineering*, Vol. 45 No. 2, pp. 461-471, doi: 10.1007/s40997-020-00377-2.

Mousavi Ajarostaghi, S.S., Zaboli, M., Javadi, H., Badenes, B. and Urchueguia, J.F. (2022), "A review of recent passive heat transfer enhancement methods", *Energies*, Vol. 15 No. 3, p. 986, doi: 10.3390/en15030986.

Mozafarie, S.S. and Javaherdeh, K. (2019), "Numerical design and heat transfer analysis of a non-Newtonian fluid flow for annulus with helical fins", *Engineering Science and Technology, an International Journal*, Vol. 22 No. 4, pp. 1107-1115, doi: 10.1016/j.jestch.2019.03.001.

Mukesh Kumar, P.C. and Hariprasath, V. (2020), "A review on triple tube heat exchangers", *Materials Today: Proceedings*, Vol. 21, pp. 584-587, doi: 10.1016/j.matpr.2019.06.719.

Myhan, R., Białobrzewski, I. and Markowski, M. (2012), "An approach to modeling the rheological properties of food materials", *Journal of Food Engineering*, Vol. 111 No. 2, pp. 351-359, doi: 10.1016/j.jfoodeng.2012.02.011.

Pagliarini, L., Bozzoli, F., Cattani, L. and Rainieri, S. (2024a), "Morphological optimization of butterfly-shaped inserts for heat transfer enhancement in tubular heat exchangers: a numerical study", *Journal of Physics: Conference Series*, Vol. 2766 No. 1, p. 12185, doi: 10.1088/1742-6596/2766/1/012185.

Pagliarini, L., Bozzoli, F., Fallahzadeh, R. and Rainieri, S. (2024b), "Non-Newtonian convective heat transfer in annuli: numerical investigation on the effects of staggered helical fins", *Fluids*, Vol. 9 No. 12, p. 272, doi: 10.3390/fluids9120272.

Rainieri, S. and Pagliarini, G. (2002), "Convective heat transfer to temperature dependent property fluids in the entry region of corrugated tubes", *International Journal of Heat and Mass Transfer*, Vol. 45 No. 22, pp. 4525-4536, doi: 10.1016/S0017-9310(02)00156-4.

Rhie, C.M. and Chow, W.L. (1983), "Numerical study of the turbulent flow past an airfoil with trailing edge separation", *AIAA Journal*, Vol. 21 No. 11, pp. 1525-1532, doi: 10.2514/3.8284.

Rios-Iribe, E.Y., Cervantes-Gaxiola, M.E., Rubio-Castro, E., Ponce-Ortega, J.M., González-Llanes, M.D., Reyes-Moreno, C. and Hernández-Calderón, O.M. (2015), "Heat transfer analysis of a non-Newtonian fluid flowing through a circular tube with twisted tape inserts", *Applied Thermal Engineering*, Vol. 84, pp. 225-236, doi: 10.1016/j.applthermaleng.2015.03.052.

Sawale, M., Benyathiar, P., Coronel, P., Rawat, A., Simunovic, J., Ozadali, F. and Mishra, D.K. (2024), "Aseptic microwave sterilization and validation of food containing particles", *Food and Bioproducts Processing*, Vol. 143, pp. 28-35, doi: 10.1016/j.fbp.2023.10.001.

Schlichting, H. and Gersten, K. (2017), *Boundary-Layer Theory*, Springer, Berlin, Heidelberg.

Schnöing, L., Augustin, W. and Scholl, S. (2020), "Fouling mitigation in food processes by modification of heat transfer surfaces: a review", *Food and Bioproducts Processing*, Vol. 121, pp. 1-19, doi: 10.1016/j.fbp.2020.01.013.

Sikorski, Z.E. (2006), *Chemical and Functional Properties of Food Components*, CRC press, Boca Raton.

Solano, J.P., Martínez, D.S., Vicente, P.G. and Viedma, A. (2023), "Enhanced thermal-hydraulic performance in tubes of reciprocating scraped surface heat exchangers", *Applied Thermal Engineering*, Vol. 220, p. 119667, doi: 10.1016/j.applthermaleng.2022.119667.

Tiwari, A.K., Javed, S., Oztop, H.F., Said, Z. and Pandya, N.S. (2021), "Experimental and numerical investigation on the thermal performance of triple tube heat exchanger equipped with different inserts with WO3/water nanofluid under turbulent condition", *International Journal of Thermal Sciences*, Vol. 164, p. 106861, doi: 10.1016/j.ijthermalsci.2021.106861.

Tonyali Karsli, G. and Cekmecelioglu, D. (2023), "3 – Design and simulation of heat exchangers for the food industry", in Jafari, S.M. (Ed.), *Thermal Processing of Food Products by Steam and Hot Water*, Woodhead Publishing, pp. 67-108, doi: 10.1016/B978-0-12-818616-9.00012-2.

Triki, R., Djemel, H. and Baccar, M. (2021), "Numerical investigation of heat treatment of an olive paste within a scraped surface heat exchanger equipped with helix screw", *Arabian Journal of Geosciences*, Vol. 14 No. 21, p. 2180, doi: 10.1007/s12517-021-08535-9.

Vocale, P., Bozzoli, F., Mocerino, A. and Rainieri, S. (2019), "Direct numerical simulation applied to the analysis of the convective heat transfer enhancement in an arc-shaped wall corrugated tube", *Computational Thermal Sciences: An International Journal*, Vol. 11 No. 4, pp. 315-325.

Zimparov, V.D., Bonev, P.J. and Hristov, J.Y. (2024), "New insight into the heat transfer and pressure drop correlations for laminar and turbulent flow in a circular tube with a twisted-tape insert: a discriminated dimensional analysis", *International Journal of Heat and Mass Transfer*, Vol. 221, p. 125072, doi: 10.1016/j.ijheatmasstransfer.2023.125072.

Corresponding author
Sara Rainieri can be contacted at: sara.rainieri@unipr.it